UNIVERSITY *of York*

This is a repository copy of *Changes in holopelagic Sargassum spp. biomass composition across an unusual year*.

White Rose Research Online URL for this paper:
https://eprints.whiterose.ac.uk/212898/

Version: Accepted Version

Article:

White Rose
university consortium
Universities of Leeds, Sheffield & York

eprints@whiterose.ac.uk
https://eprints.whiterose.ac.uk/

PNAS

Carla Botelho Machado[a,2], Robert Marsh[b,2], Jessica K. Hargreaves[c] Hazel A. Oxenford[d], Gina-Marie Maddix[e], Dale F. Webber[e], Mona Webber[f], Thierry Tonon[a,1]

[a]Centre for Novel Agricultural Products (CNAP), Department of Biology, University of York, Heslington, United Kingdom

[b]School of Ocean and Earth Science, University of Southampton, Southampton, United Kingdom

[c]Department of Mathematics, University of York, York, Heslington, United Kingdom,

[d]Centre for Resource Management and Environmental Studies (CERMES), University of the West Indies, Cave Hill, Barbados

[e]Centre for Marine Sciences, 1 Anguilla, Close, University of the West Indies, Mona, Jamaica

[f]Department of Life Sciences, 2 Anguilla Close, University of the West Indies, Mona, Jamaica

[1]Corresponding author name. Thierry Tonon. Centre for Novel Agricultural Products, Department of Biology, University of York, Heslington, York YO10 5DD, United Kingdom.

Email: thierry.tonon@york.ac.uk

[2]Both authors contributed equally to this work.

This PDF file includes:

Main Text
Tables 1 to 2

Abstract

2021 marked a decade of holopelagic sargassum (morphotypes *S. natans* I, VIII, and *S. fluitans* III) stranding on the Caribbean and West African coasts. Beaching of millions of tonnes of sargassum negatively impacts coastal ecosystems, economies, and human health. Additionally, the La Soufrière volcano erupted in St. Vincent in April 2021, at the start of the sargassum season. We investigated potential monthly variations in morphotype abundance and biomass composition of sargassum harvested in Jamaica, and assessed the influence of processing methods (shade-drying vs frozen samples) and of volcanic ash exposure on biochemical and elemental components. *S. fluitans* III was the most abundant morphotype across the year. Limited monthly variations were observed for key brown algal components (phlorotannins, fucoxanthin, and alginate). Shade-drying did not significantly alter the contents of proteins, but affected levels of phlorotannins, fucoxanthin, mannitol and alginate. Simulation of sargassum and volcanic ash drift combined with age statistics suggested that sargassum potentially shared the surface layer with ash for ~50 days, approximately 100 days before stranding in Jamaica. Integrated elemental analysis of volcanic ash, ambient seawater and sargassum biomass showed that algae harvested from August had accumulated P, Al, Fe, Mn, Zn and Ni, probably from the ash, and contained less As. This ash fingerprint confirmed the geographical origin and drift timescale of sargassum in a novel way. Since environmental conditions and processing methods influence biomass composition, efforts should continue to improve understanding, forecasting, monitoring and valorising sargassum, particularly as strandings of sargassum show no sign of abating.

Significance Statement

Since 2011, Caribbean and West African countries have been affected by millions of tonnes of stranding holopelagic sargassum. This impacts coastal ecosystems, economies and human health. Sargassum biomass harvested in Jamaica throughout 2021 shows seasonal changes in morphotype abundance, and limited variation in biochemical composition. For valorisation, shade-drying vs freeze-drying decreased phlorotannin, fucoxanthin, and alginate contents, but not total proteins. 2021 was also marked by the La Soufrière volcanic eruption in the Caribbean. We suggest that floating sargassum and volcanic ash shared the sea surface for ~50 days, approximately 100 days before reaching Jamaica, and this impacted the elemental composition of stranded biomass. This observation gives new insights on assimilation of elements by sargassum under different influences, like volcanic ash.

Main Text

Introduction

      Over the last two decades, there has been an increasing number of reports describing seaweed (macroalgae) invasions and blooms affecting coastal environments and populations worldwide (1). These seaweed events have become more frequent and impactful as the Anthropocene unfolds, with no sign of abating. They have a wide impact on coastal biodiversity and communities, and can exacerbate important socio-economic and health problems (2). One example of recent and now recurrent seaweed bloom events is the Great Atlantic Sargassum Belt (GASB) (3), caused by floating mats of holopelagic sargassum species (brown algae). Since 2011, annual stranding of millions of tonnes of sargassum biomass has become a new normal in the Caribbean and West Africa (4). Several hypotheses have been suggested to explain the emergence and recurrence of these sargassum events, including physical (5) and chemical (6) drivers associated with climate change and variability across the Tropical Atlantic (7).

      This holopelagic sargassum (referred to as sargassum hereinafter) biomass is formed by assemblage of the morphotypes *S. natans* I, *S. natans* VIII, and *S. fluitans* III (8, 9). It represents an important element in carbon cycling and sequestration at the local scale (10). In the initial years of sargassum events, the stranded biomass was seen as a waste and most of it was discarded in landfills. However, in recent years, several directions have been explored for its

85 valorisation (11), including the production of bioenergy as liquid fuels (12, 13) and biogas (14, 15,
86 16), bioremediation (17), and for soil amelioration (18, 19). Sargassum events are still considered
87 as an emergent risk (20), and progress has been made regarding governance and management
88 policies (21). One of the important parameters to consider for the implementation of valorisation
89 through industrial processes is potential changes in biomass composition depending on
90 processing methods, as feedstock needs to be stabilized before subsequent uses. In line with
91 this, we have previously explored the impact of sample processing (frozen vs sun-dried
92 sargassum) using biomass harvested during the summer 2020 in Jamaica (22). This study
93 showed that this aspect of the valorisation chain had a significant impact on some of the key
94 biochemical compounds of the sargassum that are also important for the support of its
95 commercial applications, including alginate, fucoxanthin, and phenolics. Another potential issue is
96 the consistency of the feedstock and potential seasonal variations (23). Stable value chains
97 require predictable inputs of biomass combined with a high content of the desired constituents,
98 e.g. alginates that can be used as thickening agents in different industries, or bioactive
99 compounds (e.g. fucoxanthin) that can be used in functional food (nutraceuticals) or in cosmetics.
100 The EU-Roadmap for the blue economy reported that the seasonal variations in biomass
101 composition is a characteristic of seaweeds that can affect the scalability of production and the
102 logistical processes (24). In the last few years, there have been increasing reports on seasonal
103 variations of the biochemical (25, 26, 27) and elemental (28, 29, 30) composition of sargassum,
104 as well as on seasonal changes in the morphotype abundance (31, 32, 33, 34, 35).
105   Our focus here is on the 2021 sargassum season, during which a substantial bloom was
106 evident across the Equatorial Atlantic from spring. This bloom was potentially exposed to the
107 major eruption of La Soufrière volcano, located on the island of St Vincent, which persisted for
108 around ten days from 9th of April 2021. The eruption produced an extensive plume at high altitude
109 that dispersed and deposited ash eastward, as predicted in previous atmospheric simulations
110 (36) and subsequently observed through April 2021 (37). Considering the transport pathways of
111 sargassum, the ash deposition pattern had the potential to impact Caribbean-bound sargassum.
112 Volcanic ash fertilization of the surface ocean has previously been observed in situ in the iron-
113 limited extra-tropics in the northeast Pacific following eruption of the Kasatochi volcano in the
114 Aleutian island-arc in August 2008 (38), and in the sub-polar North Atlantic after the spring 2010
115 Eyjafjallajökull volcanic eruption in Iceland (39). These natural fertilization events were associated
116 with massive and temporary increase of phytoplankton biomass. However, no study has as yet
117 investigated the potential impact of volcanic ash on the biochemical and elemental composition of
118 floating seaweeds.
119   In this context, the current study had three main objectives: (i) to investigate potential
120 seasonal changes in the morphotype abundance, as well as in the biochemical and elemental
121 composition of beached sargassum; (ii) to assess how the processing of seaweed may affect the
122 consistency of the feedstock; (iii) to determine if sargassum mats have been in contact with
123 volcanic ash, and how this may have influenced their biochemical and elemental composition.
124
125

Results

127

Satellite observations at regional scale. Areas of sargassum over the annual cycle were
129 aggregated for eight selected sub-regions by sampling FA_density data (Fig. 1). The three sub-
130 regions of the Central Atlantic (Fig. 1A-C) follow previous analysis (5), and were motivated by
131 broad separation of dynamical regimes. The East Caribbean region is split into East, Central and
132 West sub-regions (Fig. 1D-F). The south and north of Jamaica (Fig. 1G, H) were separately
133 considered following previous forecasting approach (40). Data for 2021 are plotted with the thick
134 lines, alongside corresponding data for 2011-20 (thin lines), to indicate when and where
135 sargassum in 2021 was exceptionally extensive. We additionally indicate (with green shading) the
136 10-day duration of the La Soufrière eruption (9-18 April).
137   We remark here on some general features of the 2021 area coverage, relative to the
138 previous years of extensive sargassum. First, we note that the period of eruption coincided with a
139 substantial reduction in sargassum area detected in the Western Tropical North Atlantic (Fig. 1C).

140 This was likely a consequence of reduced visibility, consistent with the widespread extent of ash
141 particles in the atmosphere to the east of La Soufrière volcano. Following this period of reduced
142 visibility, areas of sargassum substantially increased in the upstream Central Equatorial North
143 Atlantic (Fig. 1A), to an extent that exceeds all previous years over days 115-125 (late April to
144 early May). Sargassum area in the Western Tropical North Atlantic likewise increased at this time
145 to a level exceeded only in 2018, leading to record mid-summer 2021 peaks through days 150-
146 155 (early June) and days 175-205 (late June to late July).
147 Turning attention to the Caribbean, we note that sargassum area remained exceptionally
148 high late into the summer of 2021, reaching and sustaining record levels over days 215-275
149 (August-September) in the East sector (Fig. 1D), most notably over days 240-275 (September) in
150 the Central sector (Fig. 1E), and to a lesser extent in the western sector (Fig. 1F). Of
151 consequence for beaching around Jamaica (Figs. 1G, 1H), areas of sargassum were relatively
152 high through late summer, more remarkably for the southern sector, where areas exceeded
153 previous records over days 250-270 (most of September). Noting the progressively later timing of
154 excessive sargassum areas, and moving from the Central Atlantic, across the Caribbean, to the
155 Jamaican region, we have considered below the associated advective timescale for drifting
156 sargassum, based on simulated forward trajectories from the vicinity of volcanic ash deposition
157 and backward trajectories from the vicinity of Jamaica.
158
159 **Simulating drift of sargassum and volcanic ash.** To examine the possible influence of volcanic
160 ash on sargassum across the Caribbean region during spring and summer of 2021, their potential
161 common drift timescales and pathways were evaluated. By comparing the likely trajectories of
162 ash and sargassum, we assessed the extent to which specific elements associated with the
163 volcanic ash would have been available to the floating biomass, hence potentially influencing the
164 biochemical and elemental composition of the floating seaweeds. Of importance was the likely
165 difference between the timescales and pathways due to ash moving with the seawater, while
166 exposed sargassum moves also in response to surface winds; this should lead to a natural and
167 progressive downstream divergence of ash and sargassum.
168 We first considered ash deposition over an idealised triangular area, based on observed
169 dispersal of the plume (37), extending from St Vincent eastward to 50ºW at 14ºN and
170 progressively southward to 6ºN (at 50ºW). We seeded this area with particles in constant
171 concentration, added over 5 days. From this triangular area, we forward-tracked both 'sargassum
172 particles', based on an initial distribution in early April 2021, subject to 1% windage, and 'ash
173 particles', identically distributed but drifting with surface currents only. All particles were tracked
174 for 180 days, sampling currents and winds for a representative model hindcast year (1988). In
175 Fig. 2, we showed the fractional coverage and age statistics for the 'sargassum' and 'ash'
176 particles. There was a notable divergence of pathways, with advection of 'sargassum' particles
177 that is more westward (Fig. 2C) compared to the north-westward advection of 'ash' particles (Fig.
178 2A). Combined with the age statistics (Fig. 2B, D), we evaluated a timescale of ~50 days over
179 which sargassum 'shared' the surface layer with ash, assuming this to remain present on the
180 same timescale.
181 To further evaluate the provenance of sargassum reaching Jamaica in late summer, we
182 back-tracked particles from this location and time, obtaining the statistics shown in Fig. 3. The
183 distribution of fractional presence in Fig. 3A clearly reveals a primary pathway via the western
184 boundary current system, from the equatorial Atlantic and through the Caribbean. The drift
185 timescale from Barbados to Jamaica was around 100 days, considering the upstream flow
186 located south of Barbados (see Fig. 3B). This pathway and timescale could be further related to
187 the potential upstream influence of ash fallout from La Soufrière volcano, as the particles were
188 back tracked from August. Considering the broad region from the Lesser Antilles to the equatorial
189 zone, mean age in the range of 90-120 days indicated that particles arriving off east Jamaica in
190 early August transited this region between early April and early May. Given the eastward
191 dispersion and deposition of ash across the same region, we suggest that the sargassum arriving
192 east of Jamaica in early August was likely exposed to ash fallout.
193 We further noted high fractional presence to the north of Jamaica, with age (days prior to
194 arrival) increasing to the west, indicating that some of the particles (hence sargassum) arriving off

195 east Jamaica may have arrived via a longer and hence slower clockwise round-island flow. These
196 particles drift westward to the south of Jamaica, almost reaching the Yucatan Channel before
197 returning to the east. This alternative pathway provided additional context for drift timescale, and
198 the extent to which sargassum may have been subject to ash fallout, if located east of the Lesser
199 Antilles prior to the eruption of La Soufrière.

201 **Changes in morphotype abundance within sargassum biomass harvested in Jamaica.**
202 Sargassum mats present in the Equatorial Tropical Atlantic Ocean are formed by the aggregation
203 of two different species represented by three distinct morphotypes: *S. natans* I, *S. natans* VIII,
204 and *S. fluitans* III. So far, no investigation of potential variations of abundance of these
205 morphotypes across a full year of inundations events in Jamaica has been conducted. Our data
206 showed clear and significant changes in the abundance of the three identified morphotypes
207 throughout the year 2021 (Fig. 4; SI Appendix, Dataset S1). *S. fluitans* III was the most abundant
208 species in all samples analysed, with values ranging between 59 and 86 % of the biomass DW.
209 Quantities of *S. natans* fluctuated significantly with *S. natans I* being the more abundant of the
210 two morphotypes all year round (13-32 % of biomass DW). *S. natans VIII* was less abundant at
211 the end of the 2021 season, with up to 10% biomass DW in September and October. Profiles
212 were very similar between May and October, June and September, and July and August.

214 **Elemental composition of La Soufrière volcanic ash and potential influence of ash**
215 **exposure on floating sargassum**. Composition of two samples of ash that had fallen on
216 Barbados on the 11th and 13th April 2021 during the main deposition event of the La Soufrière
217 volcanic eruption was analysed. Elemental content in both samples was very similar, with Al, Ca,
218 Fe, Na and Mg being the most abundant elements with amounts above 15,000 ppm (Table 1).
219   While macroalgae elsewhere in the tropics have been demonstrated to be iron-limited
220 (41), it is long established that *S. natans* and *S. fluitans* in the western North Atlantic are
221 phosphorus-limited (42), with iron-limitation not examined. The cumulative deposition of volcanic
222 ash during April may have raised the local concentrations of iron and phosphorus substantially
223 above background levels, and these elements could have been assimilated by floating
224 sargassum. To test this hypothesis, we considered background elemental concentrations in
225 seawater across the region of interest and available from the eGEOTRACES Electronic Atlas
226 (https://www.geotraces.org/geotraces-intermediate-data-product-2021/) for the Western Atlantic
227 GA02 section (43). Taking phosphate as an example, we noted from climatology that dissolved
228 inorganic phosphate in the upper ocean was well below 0.5 µmol kg^{-1} seawater in the region
229 during April (44). This corresponded to a background concentration of 0.5 µmol kg^{-1} seawater of
230 phosphorus. We then proceeded to estimate the implied concentration of phosphorus associated
231 with ash in seawater.
232   Taking a representative deposition depth of 1 cm of ash across a broad area with a
233 deposit density of 1200 kg m^{-3} (36), and a mean (averaging BM1 and BM2) phosphorus content
234 of 515 ppm (Table 2), we obtained an integral phosphorus flux (over the deposition timescale) of
235 0.01 x 1200 x 515/10^6 = 0.00618 kg m^{-2}. Assuming rapid mixing throughout an April surface
236 mixed layer in this region with representative thickness 50 m (45), this corresponds to a seawater
237 phosphorus concentration of 1.236 x 10^{-4} kg m^{-3}, or 0.1236 g m^{-3}. Taking the molar mass of
238 phosphorus (1 mole = 30.97 g) we obtain a concentration of 0.00399 mol m^{-3}; taking seawater
239 density 1023 kg m^{-3}, this amounts to 3.90 x 10^{-6} mol kg^{-1} of phosphorus in seawater, or 3.90 µmol
240 kg^{-1} for direct comparison with climatology (maximum 0.5 µmol kg^{-1}). A minimum enrichment
241 factor was thus estimated at 7.8. We concluded that the cumulative deposition of volcanic ash
242 during April may have raised the local concentration of phosphorus in the upper ocean by (at
243 least) almost an order of magnitude above background levels. Repeating this for the other trace
244 elements measured in ash and available from the eGEOTRACES atlas, we summarise the
245 estimated mixed layer concentrations for Al, Fe, Mn, Zn, Co and Ni in Table 1. On the basis of
246 these estimates, it appears that the highest potential seawater enrichment was in Fe and Al, for
247 which concentrations increased over background levels by 4-5 orders of magnitude; Mn and Co

5

248 were enriched by 3-4 orders of magnitude, followed by Zn and Ni. Whether such enrichment
249 levels are consequential for sargassum depends on both the utility and bioavailability of these
250 elements. To the extent that the elements are assimilated into growing sargassum and
251 biologically inert, they can provide information on an upstream encounter with the ash fallout, and
252 thus inform on the geographical origin and drift timescale of floating sargassum, as considered in
253 the next section.

254 **Elemental composition of stranding sargassum samples.** We performed principal component
255 analysis (PCA) to visualize the elemental content of sargassum after different processing
256 methods and across a full season of beaching. Cluster analysis supported the separation of the
257 samples into two clusters, one corresponding to those harvested in May (F/frozen, and S/shade-
258 dried), June (F and S), July (F and S) and August (S) (cluster 1), and the other grouping samples
259 collected in August (F), September (F and S), and October (F and S) (cluster 2) (SI Appendix,
260 Fig. S1). No clear distinction was observed based on the method used for the processing of the
261 samples, while discrimination was mainly supported by the month of sampling. Most of the
262 variance (PC1 = 39.6%) was attributed to sampling before or after August, likely to be considered
263 as a transition month during the year 2021. Separation along PC1 was related to differences in
264 the content of K, As and Na in the cluster 1 direction, and of Al, Ni, and Th in the cluster 2
265 direction. Within this latter cluster, the variance in PC2 direction (16.7%) supported the separation
266 between samples harvested in September (F and S) and those collected in October (F and S)
267 and August (F), and was mainly due to the differences in the content of Ba and Mn for the
268 September direction, and of Ca, Mg, Tl in the August direction.
269   To complete this analysis, a more thorough assessment of the results was conducted.
270 Only the main observations are reported here, and a more exhaustive description of these
271 results, including p-values obtained by two-way ANOVA followed by post hoc Holm-Sidak test, is
272 given in SI Appendix (Supporting Text). Analysis of the elemental composition of sargassum
273 showed significant differences in the total element content between frozen (170,069.34 ±
274 15,657.24 − 192,629.45 ± 1,608.91 ppm) and shade-dried (142,488.37 ± 1,003.70 − 187,196.53 ±
275 7,084.02 ppm) samples (SI Appendix, Dataset S2). This was clear when comparing samples
276 collected from July to October, in which the quantities of elements was constantly lower in shade-
277 dried compared to frozen samples. When looking at monthly variations in total element content
278 for each type of sample, the only significant difference for the frozen samples was observed
279 between October and September. However, among the shade-dried samples, more statistically
280 supported differences were found: higher content of elements was quantified in July compared
281 with May and June, and lower amounts in September compared with all the other months except
282 July.
283   A systematic examination of variations for individual elements quantified in sargassum
284 samples was then conducted (Fig. 5). We only considered those for which content was
285 determined to be higher than 1 ppm, so Se, Mo, Ag, Cd, Sb, Tl, Pb, Th, U and Co were excluded.
286 The most abundant elements found in seaweed samples were K, Ca, Na, and Mg, with amounts
287 above 10,000 ppm (Fig. 5A). Although significant variations were determined when comparing the
288 influence of sample processing on the total content of elements, when looking at elements
289 individually, limited statistical support was observed for the influence of processing methods,
290 except for Na, Ca, and Ni. Based on this, and to improve clarity in subsequent analysis, only key
291 statistically supported seasonal/monthly variations for the frozen samples will be described.
292   Similar variations were observed for K and Na, with higher amounts in May-June, lower in
293 August, and then an increase in September-October (Fig. 5A). For Ca, the opposite trend was
294 observed and content was higher in August compared to the other months. Among the elements
295 for which a potential enrichment of seawater by volcanic ash was suggested, P, Fe and Al were
296 quantified in a similar range and showed similar pattern of variations (Fig. 5B). Higher contents
297 were detected in August, and, in most of the cases, remained high during September and
298 October, with values above those measured in July and previous months. Similar results were
299 observed for Mn (Fig. 5C). In contrast, As content decreased between July and August-
300 September. Zn was not detected in sargassum harvested in May and June (Fig. 5D), but was
301 quantified in samples collected in July and August, with further content increase in September-

302 October. The content in Ni almost doubled between June and August, remaining above 5 ppm
303 afterwards. Similarly, higher levels of Cu and Ba were determined in September-October
304 compared to June-July.

305 **Biochemical composition of sargassum after different processing methods and across a**
306 **full season**. PCA was used to evaluate the potential influence of processing methods and
307 potential seasonal variations on biochemical parameters known to be important for the physiology
308 of brown algae, as well as being relevant for the valorisation of this biomass. Two distinct clusters
309 were observed, one containing the frozen (F) samples, and the other corresponding to the shade-
310 dried (S) samples (SI Appendix, Fig. S2). This suggests that most of the variance (PC1 = 31.5%)
311 among the samples analysed is due to the methods used to process the samples, in contrast with
312 what was observed for the elemental composition of the same samples. The separation between
313 the two clusters was due to differences between several parameters, including alginate_mono
314 that corresponds to the percentage of the total sugars accounted for by alginate (mannuronic and
315 guluronic acid), the content of fucoxanthin and phlorotannins in the direction of the F samples,
316 and by the moisture content and the amounts of mannitol and glucose in the direction of the S
317 samples. No clear trend was associated with the second component (PC2 = 28.6%), which was
318 mainly supported by the differences in the protein and ash contents in one direction, and by
319 differences in the amounts of several monosaccharides and uronic acids in the opposite direction.
320 Building on these results, a more in-depth investigation of the results was conducted, and
321 the most relevant observations are reported in this section. A more exhaustive description,
322 including p-values obtained by two-way ANOVA followed by post hoc Holm-Sidak test, is
323 presented in SI Appendix (Supporting Text). Ash produced from seaweed biomass represented
324 37-39 % of the sargassum DW in frozen samples and 33-40% in samples after shade-drying (Fig.
325 6A; SI Appendix, Dataset S3). Moisture accounted for 8-9 % and 10-14 % of biomass DW in
326 frozen and shade-dried samples respectively. Very limited differences were observed across the
327 period of sampling and between the sample processing methods for the ash and moisture
328 contents in the samples investigated.
329 Protein content ranged between 28 and 36 mg/g biomass DW in frozen samples and 29-
330 35 mg/g biomass DW in shade-dried samples (Fig. 6B; SI Appendix, Dataset S4) No significant
331 differences in the amount of proteins were determined between the two processing methods. A
332 slight decrease in the amount of proteins was observed in June compared to other months.
333 Quantities of phenolics were more variable and usually higher in the shade-dried (0.17-0.43 mg/g
334 biomass DW) compared to the frozen samples (0.22-0.27 mg/g biomass DW) (Fig. 6C; SI
335 Appendix, Dataset S5). Very limited seasonality was detected for this class of compounds.
336 Contents in phlorotannins were systematically lower in shade-dried (0.11-0.24 mg/g biomass DW)
337 compared to frozen (0.22-0.32 mg/g biomass DW) samples (Fig. 6C; SI Appendix, Dataset S5).
338 Seasonal variations were observed only in the shade-dried samples, in particular a higher content
339 in September-October compared to May-June-July. The amounts of the pigment fucoxanthin
340 were significantly higher in frozen samples (743-1130 µg/g biomass DW) compared to shade-
341 dried samples (33-54 µg/g biomass DW) (Fig. 6D; SI Appendix, Dataset S6). There were also
342 clear seasonal variations in the frozen samples with higher contents in August-September-
343 October compared to June-July, as suggested by PCA.
344 One of the trademarks of brown algae is the prevalence of peculiar complex
345 polysaccharides and their monosaccharide composition. The total content of monosaccharides
346 ranged between 142-183 and 113-205 mg/g biomass DW in frozen and shade-dried samples
347 respectively (Fig. 6E; SI Appendix, Dataset S7). No clear trend was identified when assessing the
348 impact of processing methods on the quantities of monosaccharides between frozen and shade-
349 dried samples. In addition, no statistically supported seasonal variations were observed when
350 comparing all the frozen samples. After shade-drying, only an increased amount of
351 monosaccharides in September was observed when compared to all other months (except
352 June).The most abundant monosaccharides were the mannuronic (M) and guluronic (G) acids,
353 which are the sub-units of the cell wall polysaccharide alginates. M content ranged between 69
354 and 89 mg/g and between 43 and 87 mg/g of biomass DW for the frozen and shade-dried
355 samples respectively. For G, a wider range was observed in shade-dried (15-36 mg/g biomass

DW) compared to frozen samples (31-37 mg/g biomass DW). No specific trend was identified between the processing methods for M, while higher amounts of G were quantified in frozen compared to shade-dried sample (except for September). No monthly differences in frozen samples were monitored for both M and G. Variations were observed in shade-dried with significant higher content of M and G in September compared to other months. Alginates accounted for 10-13% and 6-12 % of the biomass DW in frozen and in shade-dried samples respectively, with usually significantly higher % in frozen compared to shade-dried samples. No statistically supported monthly variations were noticed in the frozen samples. In contrast, the shade-dried samples showed significant lower alginate % in May-July compared to June-September. The M:G ratios ranged between 2.17 and 2.41 for frozen samples, and 2.44 and 3.06 for shade-dried samples (SI Appendix, Fig. S3, and Dataset S7). Values were systematically higher in shade-dried compared to frozen samples, and no statistically supported monthly changes were observed within frozen or shade-dried samples.

Fucose is also an important monosaccharide in brown algae as a constituent (main chain or branching) of the fucose-containing sulfated polysaccharides that are a key component of the brown algal cell. It represented between 14 and 18 mg/g biomass DW in frozen samples, and 12-26 mg/g biomass DW in shade-dried samples. Content of this monosaccharide was generally higher in the latter, as statistically supported in June and September. Seasonal variations were observed only in shade-dried samples, in particular when comparing September with all other months (except June). The polyol (sugar alcohol) mannitol is a form of carbon storage produced from photosynthesis, and is also involved in the physiological response triggered in brown algae under abiotic stress conditions. Higher quantities were measured in shade-dried (13-18 mg/g biomass DW) compared to frozen samples (2-14 mg/g biomass DW). Differences were statistically supported for the months July, September, and October. Seasonal variations were observed only in frozen samples, with statistical support for comparison between months with the lowest contents (July, September, October) and those with the higher amounts (May and June). Glucose is found in the cell wall polysaccharide cellulose and in the carbon storage polysaccharide laminarin. It accounted for 4 to 6 mg/g biomass DW in frozen samples, and 3 to 10 mg/g biomass DW in shade-dried samples. Amounts of glucose were frequently higher in shade-dried samples, with significant differences for biomass harvested in May and June. No monthly differences were identified in the frozen samples. However, more glucose was found in shade-dried samples in May-June compared to July-August-September-October. Other less abundant monosaccharides and uronic acids (galactose, xylose, mannose, rhamnose, arabinose, glucuronic acid and galacturonic acid) are discussed in SI Appendix (Supporting Text).

Potential interactions between biochemical and elemental composition. To explore possible interplay between the content of biochemical compounds and of elements, a correlation analysis was conducted using results obtained for the frozen/freeze-dried samples. Focusing on biochemical compounds, we found strong correlations between mannuronic, guluronic, glucuronic galacturonic acids and mannose (SI Appendix, Fig. S4). Contents in fucose, xylose, mannose, glucose and galactose were also significantly positively correlated. Negative correlations were observed between glucuronic acid and phlorotannins/fucoxanthin, as well as between proteins and mannitol. Regarding possible interactions between the elements, content of As was strongly negatively correlated with most of the elements investigated, including Al, P, Ca, V, Mn, Fe, Co, Ni, Zn, Ag, Pb, Th, U, but positively correlated with Na and K content. Positive correlations were also observed between Mn, Fe, Co, Ni, Cu, Zn, Ba, Pb, Th, and U.

When assessing potential correlations between the content of elements and of biochemical compounds, the most interesting observations were probably the significant positive correlations between mannuronic, guluronic, and glucuronic acids and quantities of Na, K and As, and the negative correlation between these uronic acids and most of the other elements (Fig. 7). Positive correlations between As and mannuronic and guluronic acids, the constituents of the cell wall polysaccharide alginate, is in line with results obtained in the other brown alga *Laminaria digitata* in which accumulation of As was found in the cell wall and the cell membranes (46). In addition, positive correlations were observed between fucoxanthin and Mg, Al, P, Ca, Mn, Fe, Co, Ni, Cu, Ag, TI, Th, and U, and negative correlations between this pigment and Na, K, and As.

8

411 This observation suggests that fucoxanthin content may increase in response to some of these
412 elements as part of antioxidative processes (47).
413
414
415 **Discussion**
416
417 During Caribbean sargassum influxes, *S. natans* I and VIII, and *S. fluitans* III have been shown to
418 be the dominant morphotypes, and their relative abundance varied across seasons, years, and
419 regions (31, 32, 33, 34, 35). *S. fluitans* III was the predominant morphotype on the Mexican
420 Caribbean coast between September 2016 and May 2020 (31). In the same way, significant
421 seasonal variation was observed in the relative abundance of the three morphotypes of
422 sargassum in Barbados during the years 2021-2022 (34), and *S. fluitans* III was the main
423 morphotype across the sampling period considered. Our results from Jamaica obtained for 2021
424 events showed a similar trend, with *S. fluitans* III being the most abundant morphotype observed
425 after beaching, despite significant variations in relative abundance across the year. One
426 explanation for this may be related to the higher growth rates observed for *S. fluitans* III at sea
427 surface temperatures experienced within the Tropical Atlantic (i.e. > 26 °C) when compared to the
428 two *S. natans* morphotypes (48, 49, 50). It was further suggested that relative morphotype
429 composition is likely linked to seasons, meteorological and oceanographic conditions, and to the
430 oceanic sub-origins of sargassum that may vary across the year (7, 34). In light of previous
431 analysis showing some differences in the biochemical and elemental composition of individual
432 morphotypes that may be of importance for valorisation (43), we analysed potential seasonal
433 variations of stranded biomass composition, as well as influence of sample processing methods.
434 For this, we focused on several classes of compounds important for the biology and uses of
435 brown algae, and that we have already investigated in sargassum biomass, i.e. proteins,
436 phenolics, phlorotannins, fucoxanthin, monosaccharides and uronic acids (22, 51, 52).
437 No significant difference in the content of proteins was observed between frozen and
438 shade-dried samples. Similar results were obtained when comparing sun-dried and frozen
439 samples obtained for biomass harvested in the same location in Jamaica in summer 2020 (22),
440 suggesting that processing methods do not significantly alter the amount of proteins in sargassum
441 biomass. Although phenolic contents were frequently higher in shade-dried compared to frozen
442 samples, results were difficult to interpret due to variations among some of the biological
443 replicates. A lower content of phlorotannins in shade-dried samples was observed compared to
444 frozen samples, and this is in contrast with previous results showing a higher content for these
445 compounds in sun-dried compared to frozen samples (22). To explain this, we suggest that direct
446 exposure to the sun may trigger higher phlorotannin biosynthesis than when shade-dried. For
447 fucoxanthin, shade-drying showed similar impact as sun-drying as both processing methods
448 greatly reduced the quantities of this pigment. While the total amount of monosaccharides was
449 lower in sun-dried compared to frozen samples in 2020, no clear trend was observed in the
450 current study, suggesting that shade-drying may be less detrimental for the total amount of
451 monosaccharides than sun-drying. However, higher contents of alginate were usually quantified
452 in frozen samples compared to shade-dried and sun-dried samples (22). Results obtained for
453 both fucoxanthin and alginate therefore suggest that biomass should be processed shortly after
454 harvesting to maximise extraction of these valuable compounds.
455 The eruption of the La Soufriere volcano in April 2021 provided the opportunity to
456 investigate potential assimilation of elements contained in the ash by floating sargassum. It has
457 already been reported that volcano ash can fertilise iron-limited phytoplankton, in particular
458 diatoms which share some phylogenetic history with brown algae as both are Stramenopiles (38).
459 Combined analysis of sargassum and volcanic ash drift suggests that ash and sargassum
460 overlapped for about 50 days, and that biomass arriving in Jamaica in early August was likely
461 exposed to ash fallout. The overall limited monthly variations observed in the biochemical
462 composition of sargassum harvested between May and October indicates that volcanic ash
463 exposure had limited impact on the content of key compounds found in brown algal biomass. This
464 is in contrast with observations made when focusing on elemental composition. We have
465 calculated that volcanic ash had the potential to increase local seawater concentrations of P, Al,

466 Fe, Mn, Zn, Co and Ni. When examining the elemental composition of sargassum biomass
467 beaching in Jamaica across the full 2021 year, with a focus on frozen samples, we observed
468 significant increase in the content of P, Al, Fe, Mn, Zn and Ni in algal samples harvested from
469 August. We also noticed a significant decrease of As content in sargassum biomass beaching
470 after July. Nevertheless, concentrations of this metalloid remained above maximum limits
471 permitted for several potential applications of sargassum biomass including seaweed-derived
472 meal and feed in Europe (40 µg/g DW) (53), and for agricultural soils in different countries (15–50
473 µg/g DW) (28). In plants, both phosphate and arsenic, owing to their structural similarity, are
474 taken up through the same mechanisms (54). In line with this, and as observed in the samples
475 analysed in our study, a negative correlation between P and As content was observed in
476 sargassum samples collected at sea (55) and after stranding (56). It has also been shown in
477 diatoms that As toxicity and bioaccumulation decrease at elevated phosphate concentrations
478 (57). This suggests that floating sargassum had taken up elements provided by the volcanic ash,
479 and high concentrations were maintained during the advection of the mats from the Northern
480 Tropical Atlantic to Jamaica. This elemental signature, apparent in sargassum after approximately
481 3-4 months of travel from the volcanic fallout area to Jamaica, also supports that the sargassum
482 biomass has remained alive and afloat and has not suffered significant mortality or sinking out of
483 the surface layer over this time-period. This is important information, given that little or nothing is
484 known about the longevity of sargassum thalli, especially in the Tropical Atlantic.
485
486
487 **Conclusion**
488
489 In line with other recent studies in the Tropical Atlantic, *S. fluitans* III was consistently the
490 dominant morphotype beaching in Jamaica from the Great Atlantic Sargassum Belt in 2021.
491 Overall, the biochemical composition of sargassum in 2021 was quite homogenous throughout
492 the year, showing no major seasonal variations, and no apparent impact from exposure to
493 volcanic ash, except for the pigment fucoxanthin. This is important for valorisation as consistency
494 of feedstock is an important factor to consider for developing applications. In addition, changes in
495 the biochemical composition observed between processing methods should be taken into
496 consideration for the implementation of valorisation pathways. Sargassum exposed to volcanic
497 ash from La Soufriere volcano did show an increase in the elemental content of P, Al, Fe, Mn, Zn,
498 Ni, and a decrease in As. However, As levels remained high enough to hamper some potential
499 routes for uses of this biomass. In the future, it is important to continue monitoring over the long
500 term morphotype abundance, as well as biochemical and elemental biomass composition, not
501 only for valorisation, but also to assess the effect of atmosphere and ocean changes on the
502 biology and ecology of sargassum.
503
504
505 **Materials and Methods**
506
507 **Remote sensing of sargassum at regional scale**. To estimate the areal extent of sargassum in
508 selected sub-regions, satellite images provided by the Optical Oceanography Laboratory at the
509 University of South Florida via their website (https://optics.marine.usf.edu) were used. Daily maps
510 of floating algae, 'FA_density', were provided as the mean of the seven past days (including the
511 current day) following method previously described (58). FA_density images were assessed for
512 three standardised regions: the Central Atlantic Region (38-63°W, 0-22°N); the Eastern
513 Caribbean (60-75°W, 10-23°N); around Jamaica (75-82°W, 15-22°N).
514
515 **Simulation of sargassum and of volcanic ash drift.** To trace the source of sargassum arriving
516 near Jamaica, virtual 'particles', which are subject to the winds and ocean currents of an eddy-
517 resolving ocean model hindcast, were used. This hindcast dataset comprises 5-day averages of
518 surface winds and currents over 1988-2010, obtained with the Nucleus for European Modelling of
519 the Ocean (NEMO) ocean model (59) in eddy-resolving global configuration (ORCA12),
520 henceforth NEMO-ORCA12. The ORCA12 configuration of NEMO has a horizontal resolution at

521 the Equator of 1/12º, or 9.277 km, close to the resolution in previous sargassum drift calculations
522 (60, 61, 62), and essential to best represent the swift and narrow boundary currents that
523 dominate the region.
524   In forward tracking mode, particles are 'released' hourly for five days in a triangular area
525 representative of ash deposition to the east and south of St Vincent, with subsequent positions
526 recorded at daily intervals for 90 days. The particle trajectories are calculated using the off-line
527 Lagrangian ARIANE mass-preserving algorithm (63) in 'qualitative mode', with the 5-day mean
528 horizontal velocity fields of NEMO-ORCA12. ARIANE is based on an analytical solution for
529 curvilinear particle trajectories across model grid cells. In this study, particles are constrained to
530 drift with surface currents and the trajectories are hence 2-dimensional in the latitude-longitude
531 plane. As in previous studies of sargassum drift (64, 65, 66), the surface-drifting particles
532 representative of sargassum are also subject to 'windage', here specified as 1%. Particles
533 representative of ash are not subject to windage, which is hence specified as 0%.
534   Back-tracking particles for up to 120 days from just east of Jamaica (prior to beaching,
535 subject to 1% windage), we further assess the extent to which sargassum beaching in south
536 Jamaica may be potentially influenced by ash from La Soufrière. Particle data from forward and
537 back-tracking experiments are statistically analysed on a grid of resolution 0.5º x 0.5º for
538 fractional presence (number of particle transitions through a grid cell divided by total number of
539 transitions) and mean age (days adrift, since the experiment started). We run the back-tracking
540 experiment for 23 hindcast years spanning 1988-2010, to account for interannual variability in
541 winds and currents.
542
543 **Sampling of sargassum and determination of morphotype abundance.** Sargassum was
544 collected on six different occasions (May 1, June 5, July 12, August 12, September 13 and
545 October 13, 2021) from Fort Rocky Beach, Port Royal, Jamaica (17°56'13.9''N 76°49'02.8''W).
546 The algal biomass was obtained by wading into the surf (in less than 1 m of water) and using a
547 'surf net' to collect ~7 kg portions from the water column. After transport to the laboratory and
548 cleaning of non-sargassum debris, three 2 kg portions of the freshly cleaned biomass had the
549 three dominant morphotypes (*S. natans I*, *S. natans VIII* and *S. fluitans III*) separated visually, so
550 morphotype ratios could be determined. The separated portions were spread to dry in the shade
551 where daytime temperatures ranged from 28.2 to 32.5°C and night-time temperatures from 25.0
552 to 27.2 °C. The material was allowed to shade-dry for 36 hours after which each sub-sample's
553 morphotypes were weighed, recombined and packaged for shipment. In addition, three 100 g
554 portions of the unseparated biomass were packaged in separate Ziploc® bags, frozen using
555 liquid nitrogen within two hours of packaging, and stored at -20 °C. All fresh sample processing
556 was complete within three hours of collecting from the sea. Frozen samples were then freeze-
557 dried for 48 h in a Heto Power Dry PL3000 freeze dryer (Thermo Fisher Scientific). Both frozen
558 and sun-dried samples were milled to 1 mm diameter particle size using a SM 300 cutting mill
559 (Retsh), and stored before subsequent analysis.
560
561 **Sampling of volcanic ash.** Two samples of ash that had fallen on Barbados from 11-13 April
562 2021 during the main deposition event were analysed. Sample 1 was collected on the 11th of April
563 2022 and sample 2 on the 13th of April 2022 in Barbados, GPS coordinates 13°09'13.6"N
564 59°36'52.0"W.
565
566 **Elemental analysis of seaweed and volcanic ash samples.** Approximately 0.1 g of dried
567 sargassum samples was digested using a CEM MARS 6 microwave digest system in 5 ml of
568 concentrated sub-boiled nitric acid at 200 °C for 15 minutes and then diluted with Milli-Q water
569 before being sub-sampled and further diluted to give an overall dilution of approximately 2100 for
570 further inductively coupled plasma mass spectrometry analysis. The resulting samples were
571 spiked to give an In and Re final concentration of 5 ppb to act as internal standards. The
572 standards were made from the IV-Stock-50 Inorganic Ventures environmental Standard, and
573 were also spiked with In and Re at 5 ppb final concentrations. A suite of P standards were also
574 made from Inorganic Ventures single element P standard.

575	For the ash, approximately 0.1 g of the sample was weighed into a 15 ml Savillex Teflon
576	vial and digested in a mixture of sub-boiled concentrated nitric acid and concentrated hydrofluoric
577	acid (Romil SpA grade) sealed on a hotplate at 130 °C overnight. The digestion acid was dried off
578	and the samples re-dissolved in 6 M HCl before being dried and re-dissolved to make a mother
579	solution in ~3M HCl. A subsample was taken, dried and re-dissolved in 3% nitric acid, containing
580	5 ppb In and Re and 20 ppb Be to act as internal standards, to give a total dilution of ~4000. They
581	were then analysed against a suite of international rock standards (Jb-2, JB-3, JGb-1, BHVO2,
582	AGV-2, BCR-2, BIR-1, JG-2 and JR-2) and the same standards as mentioned above to obtain the
583	As concentration. All seaweed and ash samples were run on an Agilent 8900 TripleQuad
584	inductively coupled plasma mass spectrometer (QQQ-ICP-MS) using standard He, He-HMI and
585	Oxygen modes depending on the element of interest.
586
587	**Biochemical analysis of seaweed samples.** Contents of ash, moisture, proteins, phenolics,
588	phlorotannins, fucoxanthin, monosaccharides and alginates were determined as previously
589	described (22).
590
591	**Statistical analyses***.*
592	Statistical tests for investigating potential significance of changes in the abundance of the
593	morphotypes across the six months of sampling were conducted using SPSS Version 22.
594	Shapiro–Wilk analysis was used to test normality amongst all the parameters, and due to the
595	assumptions of the data, a univariate two-way ANOVA was performed, followed by a post hoc
596	Tukey test for all pairwise comparisons. The level of significance was set at p-value ≤ 0.05.
597	Potential variations in the biochemical and elemental composition of the biomass related
598	to months of collection and processing of samples (frozen and shade-dried) were investigated
599	following several approaches. Principal component analysis (PCA) and cluster analysis were
600	performed in RStudio on UV (unit variance)-scaled data to give all variables equal influence on
601	the analyses. Data were further analysed using SigmaPlot version 14.5. They were tested for
602	normality using the Shapiro-Wilk test and homogeneity of variance by the Brown-Forsythe test.
603	Then, two-way ANOVA was performed, followed by a post hoc Holm-Sidak test for all pairwise
604	multiple comparisons. The significance level was fixed at p-value ≤ 0.05 for all the data analyses.
605	To explore possible relationships between biochemical and elemental composition, a test
606	of association between paired samples using Pearson's product moment correlation coefficient
607	was performed using RStudio. The level of significance was set at p-value ≤ 0.05.
608

Data, Materials, and Software Availability.

The satellite datasets analysed for this study can be found at the website of the Optical Oceanography Laboratory at the University of South Florida (https://optics.marine.usf.edu), selecting 'Satellite Data Products', and further selecting: 'E. Caribbean' and 'Jamaica' from 'Caribbean'; 'Central Atlantic' from 'South America'. To download all daily FA_density images for the 'E. Caribbean', 'Jamaica' and 'Central Atlantic' regions, we used Matlab scripts that are archived on Zenodo (published with a link to this article, when a DOI is available). Ensemble primary particle tracking data, analysis programmes (Fortran) and scripts (Matlab) used to produce Figures 2 and 3 will also be archived on Zenodo, on publication. The ORCA12 hindcast dataset (archived at National Oceanography Centre, Southampton, UK) has been partly lost through disk failure subsequent to use in the drift calculations.

References
1.   R. Bermejo, L. Green-Gavrielidis, G. Gao, Macroalgal blooms in a global change context. *Front. Mar. Sci.* 10:1204117 (2023).
2.   United Nations Environment Programme-Caribbean Environment Programme, "Sargassum White Paper – Turning the crisis into an opportunity. Ninth Meeting of the Scientific and Technical Advisory Committee (STAC) to the Protocol Concerning Specially Protected Areas and Wildlife (SPAW) in the Wider Caribbean Region" (2021).
3.   M. Wang et al., The great Atlantic Sargassum belt. *Science* 365, 83-87 (2019).
4.   Y.A. Fidai, J. Dash, E.L. Tompkins, T. Tonon, A systematic review of floating and beach landing records of Sargassum beyond the Sargasso Sea. *Environ. Res. Commun.* 2, 122001 (2020).
5.   N. Skliris, M. Marsh, K.A. Addo, H.A. Oxenford, Physical drivers of pelagic sargassum bloom inter-annual variability in the Central West Atlantic over 2010-2020. *Ocean Dyn.* 72, 383-404 (2022).
6.   B.E. Lapointe et al., Nutrient content and stoichiometry of pelagic *sargassum* reflects increasing nitrogen availability in the Atlantic Basin. *Nat. Commun.* 12, 3060 (2021).
7.   R. Marsh et al., Climate-*sargassum* interactions across scales in the tropical Atlantic. *Plos Climate* 2, e0000253 (2023).
8.   A.E. Parr, Quantitative observations on the pelagic *sargassum* vegetation of the Western North Atlantic. *Bull. Bingham Oceanogr. Coll.* 6, 1–94 (1939).
9.   J.M. Schell, D.S. Goodwin, A.N.S. Siuda, Recent *sargassum* inundation events in the Caribbean: Shipboard observations reveal dominance of a previously rare form. *Oceanography* 28, 8-10 (2015).
10. C. Hu, M. Wang, B.E. Lapointe, R.A. Brewton, F.J. Hernandez, On the Atlantic pelagic Sargassum's role in carbon fixation and sequestration. *Sci. Total Environ.* 781, 146801 (2021).
11. A. Desrochers, S.-A. Cox, H.A. Oxenford, B. van Tussenbroek, "Sargassum Uses Guide: A Resource for Caribbean Researchers, Entrepreneurs and Policy Makers". Report Prepared for the Climate Change Adaptation in the Eastern Caribbean Fisheries Sector (CC4FISH) Project of the Food and Agriculture Organization (FAO) and the Global Environment Facility (GEF) (2020).
12. E. Aparicio et al., High-pressure technology for *Sargassum* spp biomass pretreatment and fractionation in the third generation of bioethanol production. *Bioresour Technol.* 329, 124935 (2021)
13. U.C., Marx, J. Roles, B. Hankamer, *Sargassum* blooms in the Atlantic Ocean – from a burden to an asset. *Algal Res.* 54, 102188 (2021).
14. T.M. Thompson, B.R. Young, S. Baroutian, S., Pelagic *Sargassum* for energy and fertiliser production in the Caribbean: a case study on Barbados. *Renew. Sust. Energ. Rev.* 118, 109564 (2020).

682 15. T.M. Thompson, B.R. Young, S. Baroutian, Enhancing biogas production from Caribbean
683   pelagic *Sargassum* utilising hydrothermal pretreatment and anaerobic co-digestion with
684   food waste. *Chemosphere* 275, 130035 (2021).
685 16. H.A. López-Aguilar et al., Practical and theoretical modeling of anaerobic digestion of
686   *Sargassum* spp. in the Mexican Caribbean. *Pol. J. Environ. Stud.* 30, 3151-3161 (2021).
687 17. S. Saldarriaga-Hernandez, G. Hernandez-Vargas, H.M.N. Iqbal, D. Barceló, R. Parra-
688   Saldívar, Bioremediation potential of *Sargassum* sp. Biomass to tackle pollution in coastal
689   ecosystems: circular economy approach. *Sci. Total Environ.* 715, 136978 (2020).
690 18. C. Trench et al., Application of stranded pelagic *sargassum* biomass as compost for
691   seedling production in the context of mangrove restoration. *Front. Environ. Sci.* 10,
692   932293 (2022).
693 19. A.A. Abdool-Ghany, C.G.L. Pollier, A.M. Oehlert, P.K. Swart, T. Blare, K. Moore, H.M.
694   Solo-Gabriele, Assessing quality and beneficial uses of *Sargassum* compost. Waste
695   Manage. 171, 545-556 (2023).
696 20. V. Dominguez Almela et al., Science and policy lessons learned from a decade of
697   adaptation to the emergent risk of *sargassum* proliferation across the tropical Atlantic.
698   *Environ. Res. Commun.* DOI 10.1088/2515-7620/acd493 (2023).
699 21. S. van der Plank et al., Polycentric governance, coordination and capacity: the case of
700   *Sargassum* influxes in the Caribbean. *Coast. Manage.* 50, 285-205 (2022).
701 22. C.B. Machado et al., Pelagic *Sargassum* events in Jamaica: Provenance, morphotype
702   abundance, and influence of sample processing on biochemical composition of the
703   biomass. *Sci. Total Environ.* 817, 152761 (2022).
704 23. H.A., Oxenford, S.-A. Cox, B.I. van Tussenbroek, A. Desrochers. Challenges of turning
705   the *sargassum* crisis into gold: current constraints and implications for the Caribbean.
706   *Phycology* 1: 27-48 (2021).
707 24. European Commission, Executive Agency for Small and Medium-sized Enterprises,
708   Sijtsma, L., Guznajeva, T., Le Gallou, M., et al., Blue Bioeconomy Forum: roadmap for
709   the   blue   bioeconomy,   Publications   Office,   2020,
710   https://data.europa.eu/doi/10.2826/605949. Last access 11.07.2023.
711 25. B.V. Nielsen et al., Chemical characterisation of *Sargassum* inundation from the Turks
712   and Caicos: seasonal and post stranding changes. *Phycology* 1, 143-162 (2021).
713 26. S. Saldarriaga-Hernandez, E. M. Melchor-Martínez, D. Carrillo-Nieves, R. Parra-Saldívar,
714   H.M.N. Iqbal, Seasonal characterization and quantification of biomolecules from
715   *Sargassum* collected from Mexican Caribbean coast - a preliminary study as a step
716   forward to blue economy. *J. Environ. Manag.* 298, 113507 (2021).
717 27. P.A. Ortega-Flores et al., Trace elements in pelagic *Sargassum* species in the Mexican
718   Caribbean: Identification of key variables affecting arsenic accumulation in *S. fluitans*,
719   *Sci. Total Environ.* 806, 150657 (2022).
720 28. R.E. Rodríguez-Martínez et al., Element concentrations in pelagic *sargassum* along the
721   Mexican Caribbean coast in 2018-2019. *PeerJ* 8, e8667 (2020).
722 29. K. Alleyne, F. Neat, H.A. Oxenford, An analysis of arsenic concentrations associated with
723   *sargassum* influx events in Barbados. *Mar. Pollut. Bull.* 192, 115064 (2023).
724 30. P.A. Ortega-Flores et al., Inorganic arsenic in holopelagic *Sargassum* spp. stranded in
725   the Mexican Caribbean: Seasonal variations and comparison with international
726   regulations and guidelines, *Aquat. Bot.* 188, 103674 (2023).
727 31. M. García-Sánchez et al., Temporal changes in the composition and biomass of beached
728   pelagic *Sargassum* species in the Mexican Caribbean. *Aquat. Bot.* 167, 103275 (2020).
729 32. R. Cabrera, J. Díaz-Larrea, A.J. Areces, L. Nuñez-García, J.R. Cruz-Aviña, R.
730   Radulovich, Registro de arribazón inusual de *Sargassum* (Phaeophyceae) para la costa
731   Atlántica de Costa Rica. *Hidrobiológica* 31, 31-42 (2021).
732 33. L.A. Iporac, D.C. Hatt, N.K. Bally, A. Castro, E. Cardet, R. Mesidor, S. Olszak, A. Duran,
733   D. A. Burkholder, L. Collado-Vides, Community-based monitoring reveals spatiotemporal
734   variation of Sargasso inundation levels and morphotype dominance across the Caribbean
735   and South Florida. *Aquat. Bot.* 182, 103546 (2022).

736 34. K.S.T. Alleyne, D. Johnson, F. Neat, H.A. Oxenford, H. Vallès, Seasonal variation in
737   morphotype composition of pelagic *Sargassum* influx events is linked to oceanic origin.
738   *Sci Rep.* 13, 3753 (2023).
739 35. E. G. Torres-Conde, B. I. van Tussenbroek, R. E. Rodríguez-Martínez, B. Martínez-
740   Daranas, Temporal Changes in the Composition of Beached Holopelagic *Sargassum*
741   spp. along the Northwestern Coast of Cuba. *Phycology* **3**, 405–412 (2023).
742 36. A.P. Poulidis et al., Meteorological controls on local and regional volcanic ash dispersal.
743   *Sci. Rep.* 8, 6873 (2018).
744 37. I.A. Taylor et al., Satellite measurements of plumes from the 2021 eruption of La
745   Soufrière, St Vincent. *Atmos. Chem. Phys. Discuss.* doi.org/10.5194/acp-2022-772
746   (2022).
747 38. B. Langmann, K. Zakšek, M. Hort, S. Duggen, Volcanic ash as fertiliser for the surface
748   ocean. *Atmos. Chem. Phys.* 10, 3891-3899 (2010).
749 39. E.P. Achterberg et al., Natural iron fertilization by the Eyjafjallajökull volcanic eruption.
750   *Geophys. Res. Lett.*, 40, 921-926 (2013).
751 40. R. Marsh et al., Seasonal predictions of holopelagic *Sargassum* across the Tropical
752   Atlantic accounting for uncertainty in drivers and processes: The SARTRAC Ensemble
753   Forecast System. *Front. Mar. Sci.* 8, 722524 (2021).
754 41. A. Anton et al., Iron deficiency in seagrasses and macroalgae in the Red Sea is unrelated
755   to latitude and physiological performance. *Front. Mar. Sci.* 5, 74 (2018).
756 42. B.E. Lapointe, Phosphorus-limited photosynthesis and growth of *Sargassum natans* and
757   *Sargassum fluitans*(Phaeophyceae) in the western North Atlantic. *Deep-Sea Res. Part A*
758   33, 391-399 (1986).
759 43. R. Middag et al., Dissolved aluminium in the ocean conveyor of the West Atlantic
760   Ocean: Effects of the biological cycle, scavenging, sediment resuspension and
761   hydrography. *Mar. Chem.* 177, 69-86 (2015).
762 44. T.P. Boyer et al., World Ocean Atlas 2018. [surface phosphate]. NOAA National Centers
763   for Environmental Information (2018). Dataset accessed 4th of April 2022.
764 45. C. de Boyer Montégut, G. Madec, A.S. Fischer, A. Lazar, D. Iudicone, Mixed layer depth
765   over the global ocean: An examination of profile data and a profile-based climatology. *J.*
766   *Geophys. Res.* 109, C12003 (2004).
767 46. E. Ender et al., Why is NanoSIMS elemental imaging of arsenic in seaweed (*Laminaria*
768   *digitata*) important for understanding of arsenic biochemistry in addition to speciation
769   information? *J. Anal. At. Spectrom.* 34, 2291-2302 (2019).
770 47. G. B. Costa et al., Physiological damages of *Sargassum cymosum* and *Hypnea*
771   *pseudomusciformis* exposed to trace metals from mining tailing. *Environ. Sci. Pollut. Res.*
772   26, 36486–36498 (2019).
773 48. M. Corbin, H.A. Oxenford, Assessing growth of pelagic *sargassum* in the Tropical
774   Atlantic. *Aquat. Bot.* 187, 103654 (2023).
775 49. E. Magaña-Gallegos et al., Growth rates of pelagic *Sargassum* species in the Mexican
776   Caribbean. *Aquat. Bot.* 185, 103614 (2023a).
777 50. E. Magaña-Gallegos et al., The effect of temperature on the growth of holopelagic
778   *Sargassum* species. *Phycology* 3, 138-146 (2023b).
779 51. D. Davis et al., Biomass composition of the golden tide pelagic seaweeds *Sargassum*
780   *fluitans* and *S. natans* (morphotypes I and VIII) to inform valorisation pathways. *Sci Total*
781   *Environ.* 762, 143134 (2021).
782 52. T. Tonon et al., Biochemical and elemental composition of pelagic *sargassum* biomass
783   harvested across the Caribbean. *Phycology* 2, 204-215 (2022).
784 53. Official Journal of the European Union, 2019. Commission regulation (EU) 2019/1869 of
785   7 November 2019 amending and correcting annex I to directive 2002/32/EC of the
786   European Parliament and of the council as regards maximumlevels for certain
787   undesirable substances in animal feed. Available at. https://eur-lex.europa.eu/legal-
788   content/EN/TXT/PDF/?uri=CELEX:32019R1869&from=EN. Last access 11.07.2023.
789 54. N. Kandhol, V.P. Singh, L. Herrera-Estrella, L.P. Tran, D.K. Tripathi, Arsenite: the umpire
790   of arsenate perception and responses in plants. *Trends Plant Sci.* 27, 420-422 (2022).

791 55. D.J. McGillicuddy, P.L. Morton, R.A. Brewton, C. Hu, T.B. Kelly, A.R. Solow, B.E.
792   Lapointe, Nutrient and arsenic biogeochemistry of *Sargassum* in the western Atlantic.
793   *Nat. Commun.* 14, 6205 (2023).
794 56. T. Gobert et al., Trace metal content from holopelagic *Sargassum* spp. sampled in the
795   tropical North Atlantic Ocean: emphasis on spatial variation of arsenic and phosphorus.
796   *Chemosphere* 308, 136186 (2022).
797 57. Q. Ma, L. Chen, L. Zhang, Effects of phosphate on the toxicity and bioaccumulation of
798   arsenate in marine diatom *Skeletonema costatum*. *Sci. Total Environ.* 857, 159566
799   (2023).
800 58. M. Q. Wang, C.M. Hu, Mapping and quantifying *Sargassum* distribution and coverage in
801   the Central West Atlantic using MODIS observations. *Remote Sens. Environ.* 183, 356-
802   367 (2016).
803 59. G. Madec, NEMO reference manual, ocean dynamic component: NEMO-OPA. Rep. 27,
804   Note du pôle de modélisation, Institut Pierre Simmon Laplace (IPSL), France, ISSN No.
805   1288-1619 (2015).
806 60. N.F. Putman, G.J. Goni, L.J. Gramer, C. Hu, E.M. Johns, J. Trinanes, M. Wang,
807   Simulating transport pathways of pelagic *Sargassum* from the Equatorial Atlantic into the
808   Caribbean Sea. *Prog. Oceanogr.* 165, 205-214 (2018).
809 61. M.T. Brooks, V.J. Coles, R.R. Hood, J.F.R. Gower, Factors controlling the seasonal
810   distribution of pelagic *Sargassum*. *Mar. Ecol. Prog. Ser.* 599, 1-18 (2018).
811 62. E.M. Johns et al., The establishment of a pelagic *Sargassum* population in the Tropical
812   Atlantic: Biological consequences of a basin-scale long distance dispersal event. *Prog.*
813   *Oceanogr.* 182, 102269 (2020).
814 63. B. Blanke, S. Raynaud. Kinematics of the Pacific Equatorial Undercurrent: An Eulerian
815   and Lagrangian approach from GCM results. *J. Phys. Oceanogr.* 27, 1038-1053 (1997).
816 64. D.R. Johnson, J.S. Franks, H.A. Oxenford, S.L. Cox, Pelagic *sargassum* prediction and
817   marine connectivity in the tropical Atlantic. *Gulf. Caribbean Res.* 31 doi:
818   10.18785/gcr.3101.15 (2020).
819 65. N.F. Putman, R. Lumpkin, M.J. Olascoaga, J. Trinanes, G.J. Goni, Improving transport
820   predictions of pelagic *Sargassum*. *J. Exper. Mar. Biol. Ecol.* 529, 151398 (2020).
821 66. L. Berline et al., Hindcasting the 2017 dispersal of *Sargassum* algae in the Tropical North
822   Atlantic. *Mar. Pollut. Bull.* 158, 111431 (2020).
823
824

Figures and Tables

Figure 1. Regionally aggregated areas (km^2) of sargassum: (A) Central Equatorial North Atlantic; (B) Central Tropical North Atlantic; (C) West Tropical North Atlantic; (D) East Caribbean – East; (E) East Caribbean – Central; (F) East Caribbean - West; (G) North of Jamaica; (H) South of Jamaica. Thick curves indicate 2021, thin curves indicate 2011-20, and green shading indicates the timing and duration of the major La Soufrière eruption (9-18 April). In (G)-(H), red vertical lines indicate the timing of beach sampling over May-October in the south of Jamaica.

Figure 2. Statistics of simulated 180-day forward trajectories from the triangular area representative of volcanic ash deposition in early April: (A,C) fractional presence; (B,D) mean age; (A,B) drifting with surface currents only (simulating ash dispersal); (C,D) drifting with surface currents and subject to 1% windage (simulating sargassum dispersal).

Figure 3. Statistics of simulated 120-day backward trajectories for August released over 1988-2010 off east Jamaica (white circle): (A) fractional presence; (B) mean age (days before arrival off Jamaica). St Vincent is indicated with a red circle.

Figure 4. Relative abundance of the three sargassum morphotypes across the 2021 season in Jamaica. Results of statistical analysis, including of post hoc test, are provided in dataset S1.

Figure 5. Elemental composition of sargassum harvested in Jamaica across the 2021 sargassum inundation season. Samples were all frozen prior to analysis. For ease of visualisation, elements were grouped by panel according to concentrations in seaweed biomass: (A) - very high, (B) - high, (C) - medium, (D) - low. The mean ± SD is reported for each measurement. Results of statistical analysis, including of post hoc test, are provided in dataset S2.

Figure 6. Biochemical composition of sargassum harvested in Jamaica across the year 2021. Results show contents in ash and moisture (A), proteins (B), phenolics and phlorotannins (C), fucoxanthin (D), and monosaccharides (E). Results of statistical analysis, including of post hoc test, are provided in dataset S3 for panel A, S4 for panel B, S5 for panel C, S6 for panel D, and S7 for panel E.

Figure 7. Heat map showing potential correlations between the contents of biochemical compounds and of elements in freeze-dried sargassum biomass harvested at different times of the year 2021. Only significant correlations (p-value ≤ 0.05) are plotted. Alginate_bio, percentage of biomass accounted for by alginate (mannuronic and guluronic acids); Alginate_mono, percentage of the total sugars accounted for by alginate (mannuronic and guluronic acids); MG_ratio, mannuronic acid:guluronic acid (M:G) ratio; Perc_DW, percentage of the dry weight accounted for by the total quantities of sugars; Total sugars, total quantities of mannitol, monosaccharides and uronic acids. An extended version of this figure is presented in Fig. S4.

Table 1. Elemental composition of ash collected in Barbados on the 11th (BM1) and the 13th (BM2) of April 2021. Only shown are elements with content > 10 ppm and As. The mean ± SD is reported for each measurement.

Elements	BM1	BM2
Al	88,359.87 ± 599.84	86,944.36 ± 1,436.78
Ca	62,171.10 ± 329.44	61,261.41 ± 509.27
Fe	51,005.63 ± 1,884.46	48,450.25 ± 784.88
Na	24,050.41 ± 245.12	24,770.91 ± 178.63
Mg	20,435.85 ± 518.77	17,673.39 ± 350.84
Ti	4,848.69± 169.45	4,824.63 ± 49.00
K	3,722.97 ± 97.436	3,963.50 ± 40.11
Mn	1,152.47 ± 20.79	1,106.06 ± 8.36
P	495.80 ± 12.13	533.75 ± 3.30
Sr	216.56 ± 1.09	220.65 ± 3.16
V	195.36± 15.10	177.61 ± 4.43
Ba	104.68 ± 2.22	112.59 ± 1.44
Cu	83.75± 0.70	93.60 ± 6.12
Zn	81.48 ± 2.10	76.06 ± 0.85
Zr	73.68 ± 2.60	78.45 ± 0.83
Cr	34.25 ± 5.82	28.78 ± 0.84
Sc	26.65 ± 0.59	24.78± 0.04
Y	22.96 ± 0.44	24.25 ± 0.25
Co	17.79 ± 0.74	16.11 ± 0.18
Ni	14.66 ± 0.836	12.32 ± 0.27
Ce	12.35 ± 0.28	13.27 ± 0.12
Rb	9.99 ± 0.30	10.77 ± 0.13
As	1.23 ± 0.04	1.35 ± 0.03

Table 2. Measured seawater and ash concentrations, and estimated enrichment factors for seven selected elements determined in both ash and sargassum, and available in the eGEOTRACES atlas for samples collected along section GA02 (https://www.geotraces.org/geotraces-intermediate-data-product-2021/).

Elements	GEOTRACES concentration in the surface mixed layer (1)	Measured mean concentration in volcanic ash (ppm)	Estimated concentration in mixed layer after ash exposure (2)	Estimated seawater enrichment factor, (2)/(1)
Al	~30 nmol kg^{-1}	87652	760 µmol kg^{-1}.	~2.5 x 10^4
Fe	~0.5 nmol kg^{-1}	49728	209 µmol kg^{-1}	~4.2 x 10^5
Mn	~2 nmol kg^{-1}	1129	4.82 µmol kg^{-1}	~2410
P	< 0.5 µmol kg^{-1}	515	3.90 µmol kg^{-1}	7.8 (minimum)
Zn	< 0.5 nmol kg^{-1}	79	0.283 µmol kg^{-1}	567 (minimum)
Co	~30 pmol kg^{-1}	17	0.142 µmol kg^{-1}	~4700
Ni	~2 nmol kg^{-1}	13.5	0.054 µmol kg^{-1}	~27

(A) Central Equatorial North Atlantic (0-10N; 38-50W)
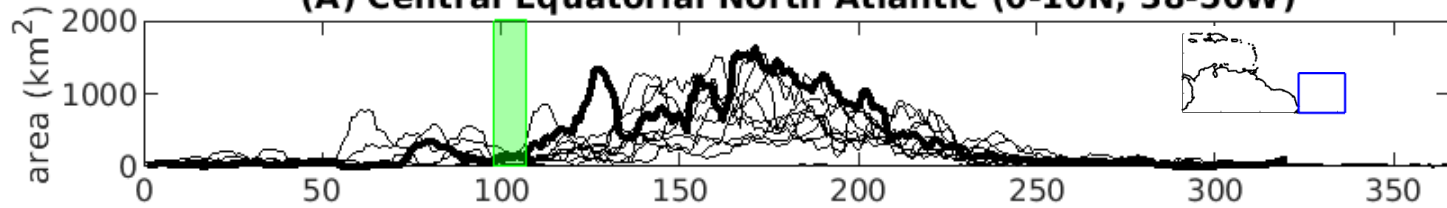
(B) Central Tropical North Atlantic (10-20N; 38-50W)
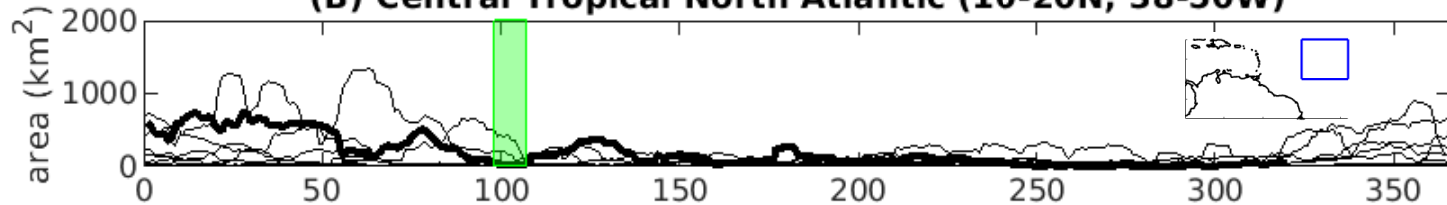
(C) West Tropical North Atlantic(6-20N; 50-63W)
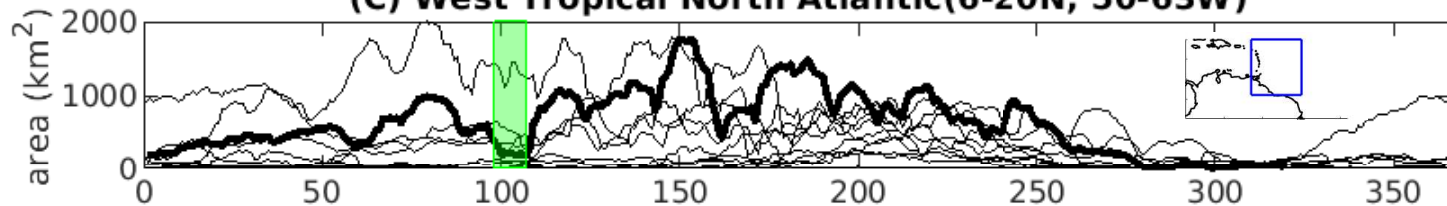
(D) East Caribbean - East (10-18N; 60-65W)
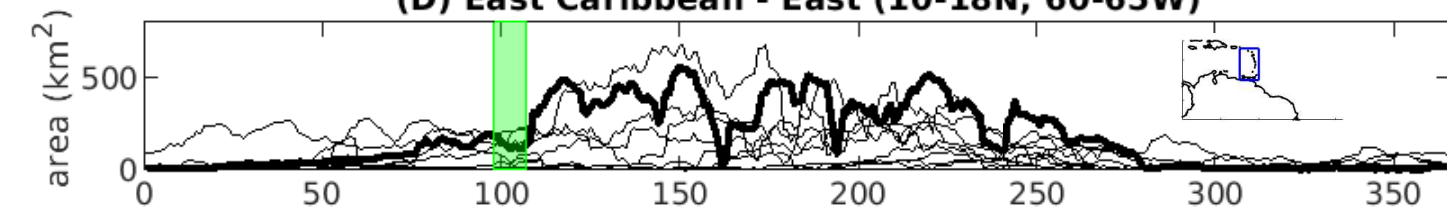
(E) East Caribbean - Central (10-18N; 65-70W)
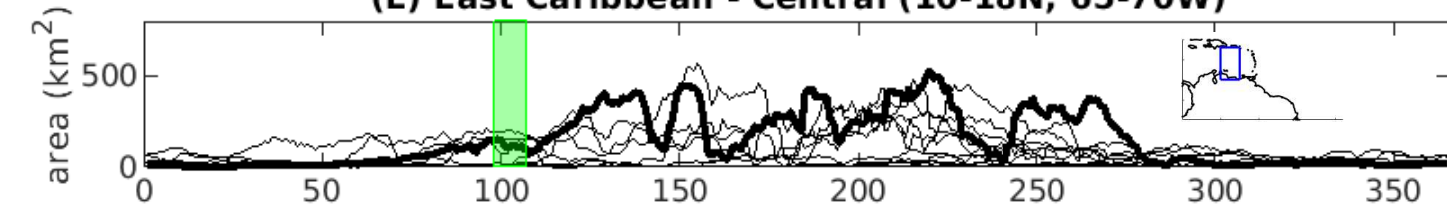
(F) East Caribbean - West (10-18N; 70-75W)
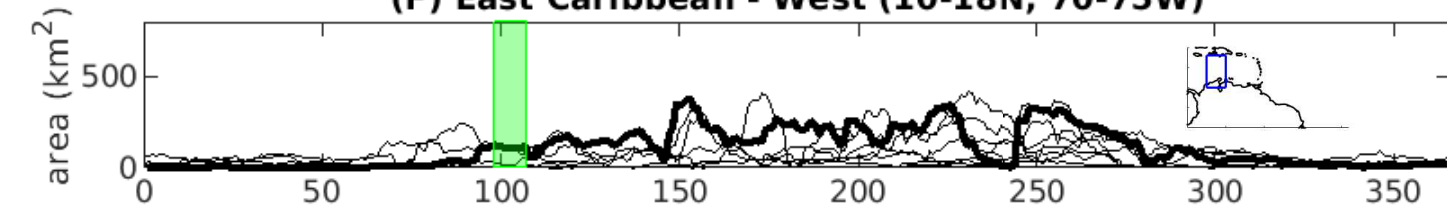
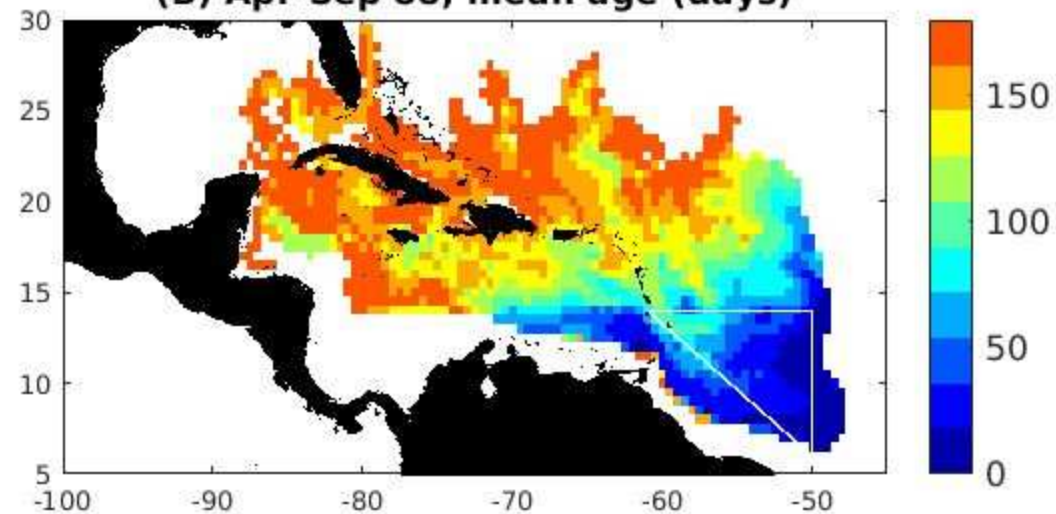(G) North of Jamaica (18-20N; 75-80W)
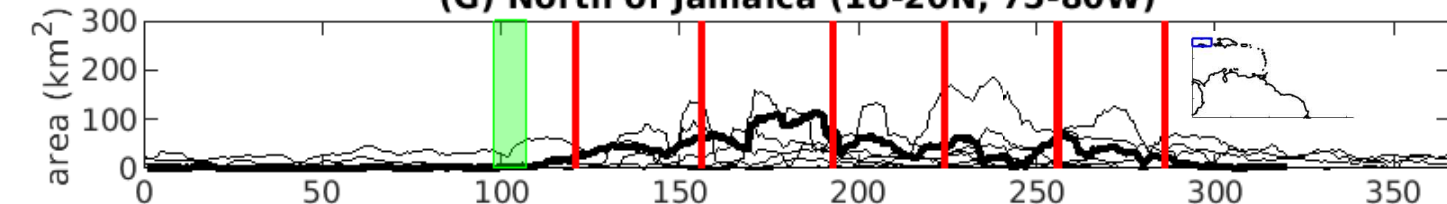
(H) South of Jamaica (16-18N; 75-80W)
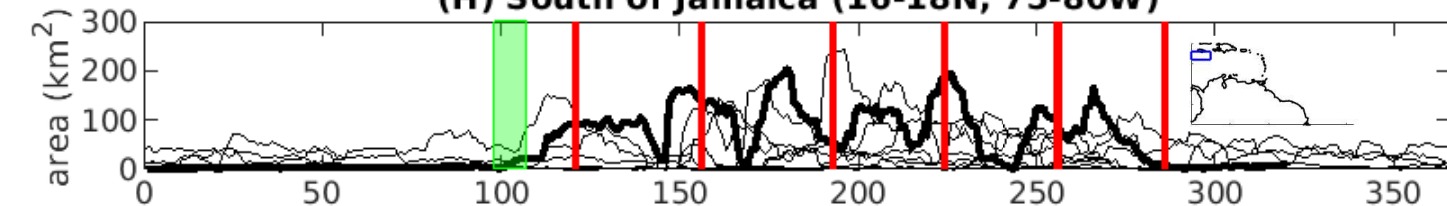
(A) Apr-Sep 88; $\log_{10}$(fraction)
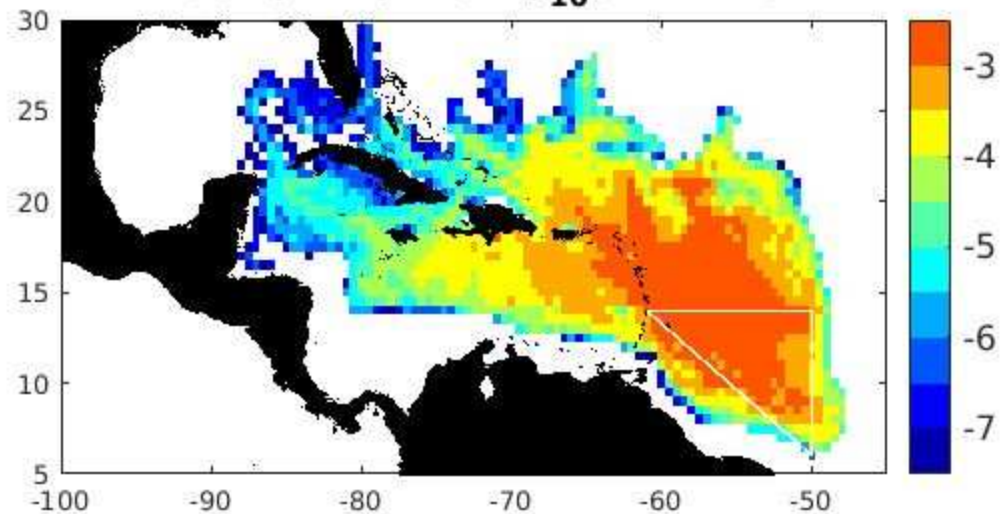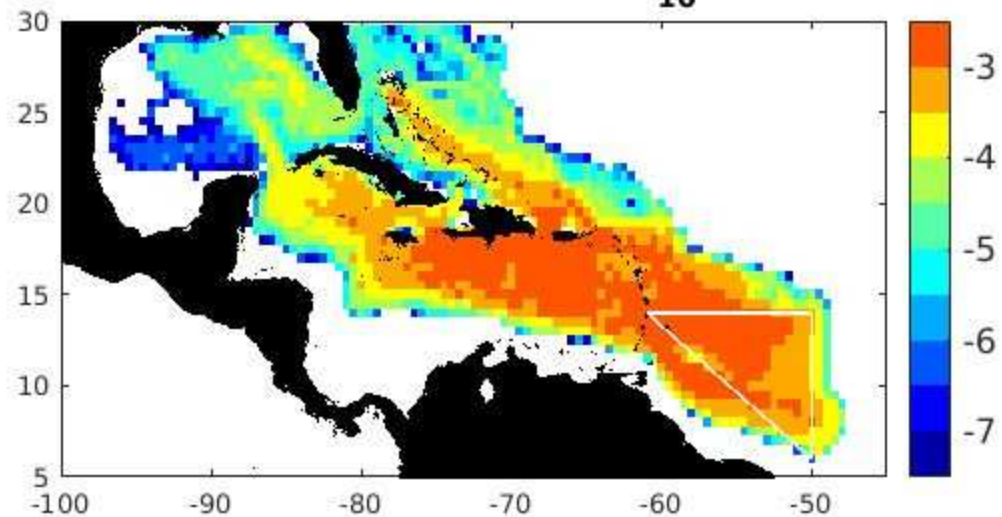
(B) Apr-Sep 88; mean age (days)

(C) Apr-Sep 88 + windage; $\log_{10}$(fraction)

(D) Apr-Sep 88 + windage; mean age (days)
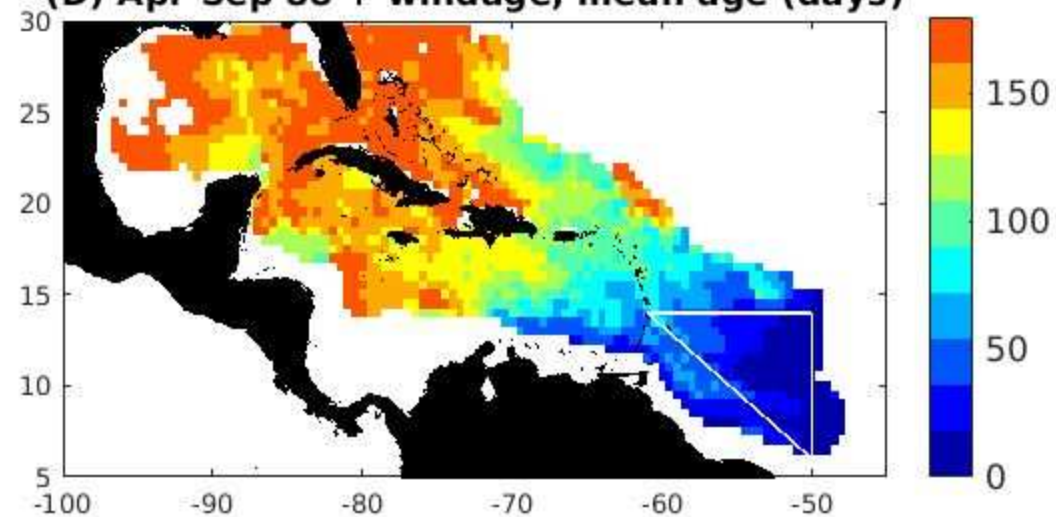
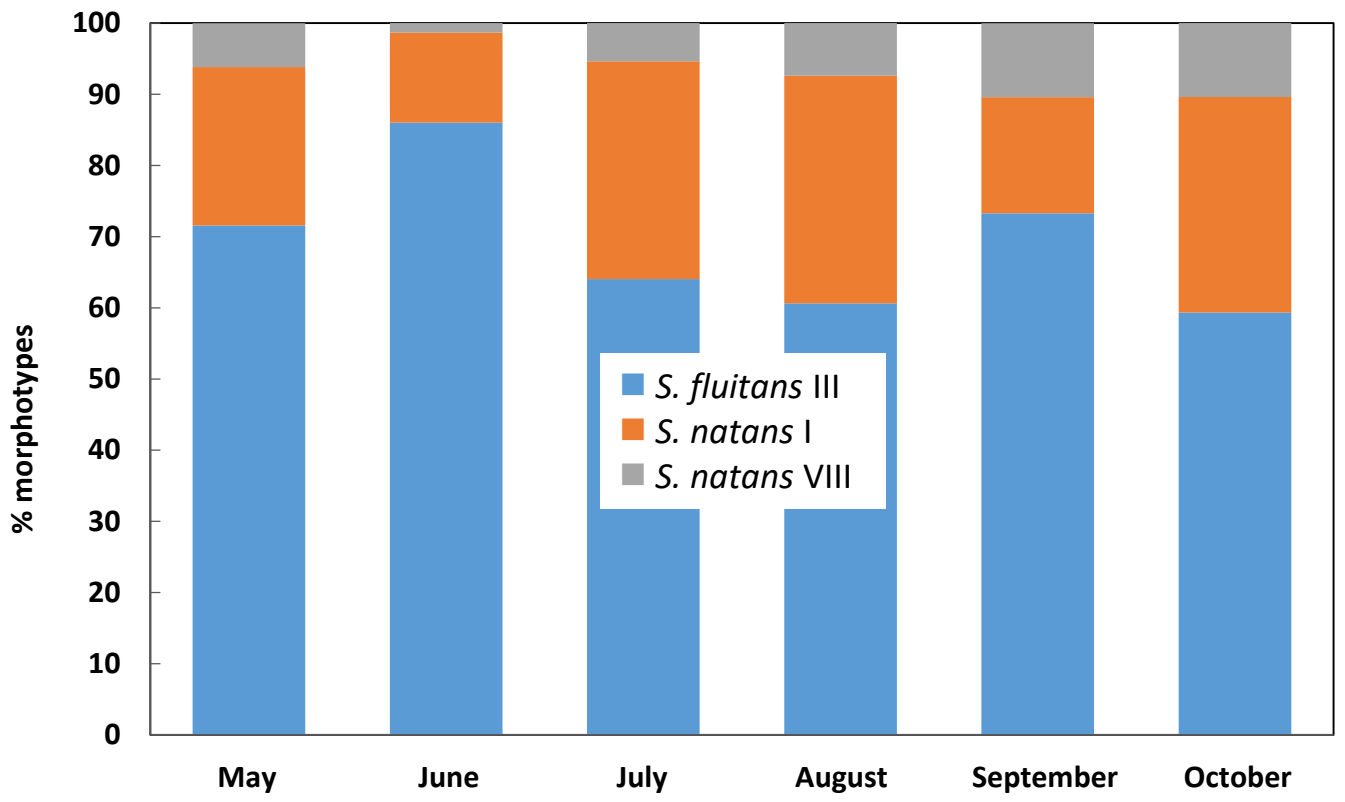**(A) from east of Jamaica; log$_{10}$(fraction)**
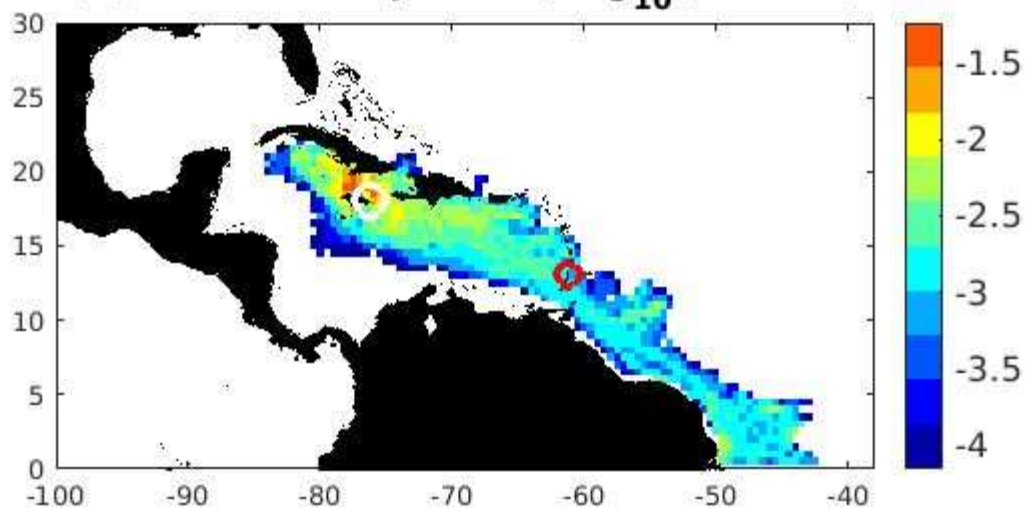
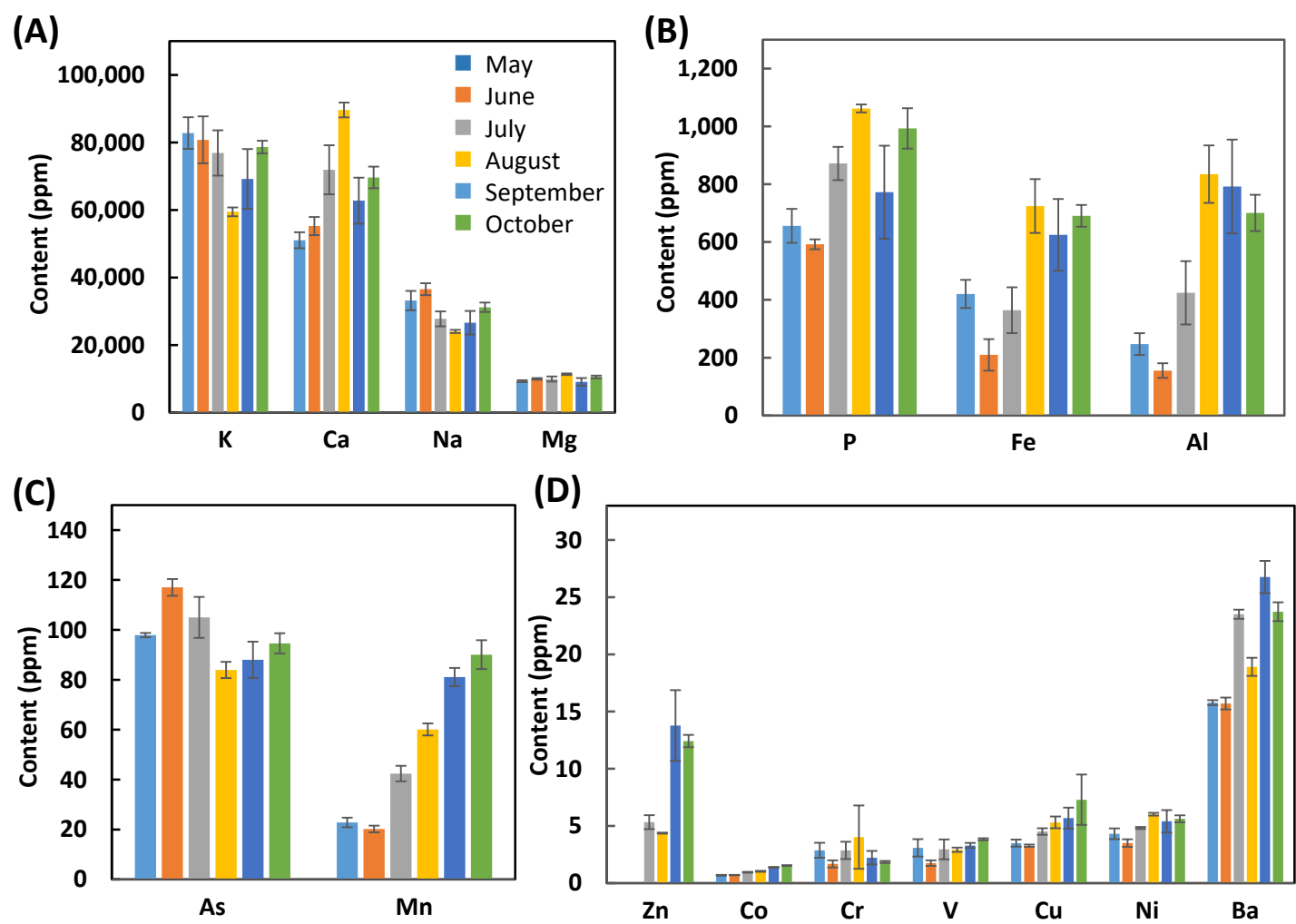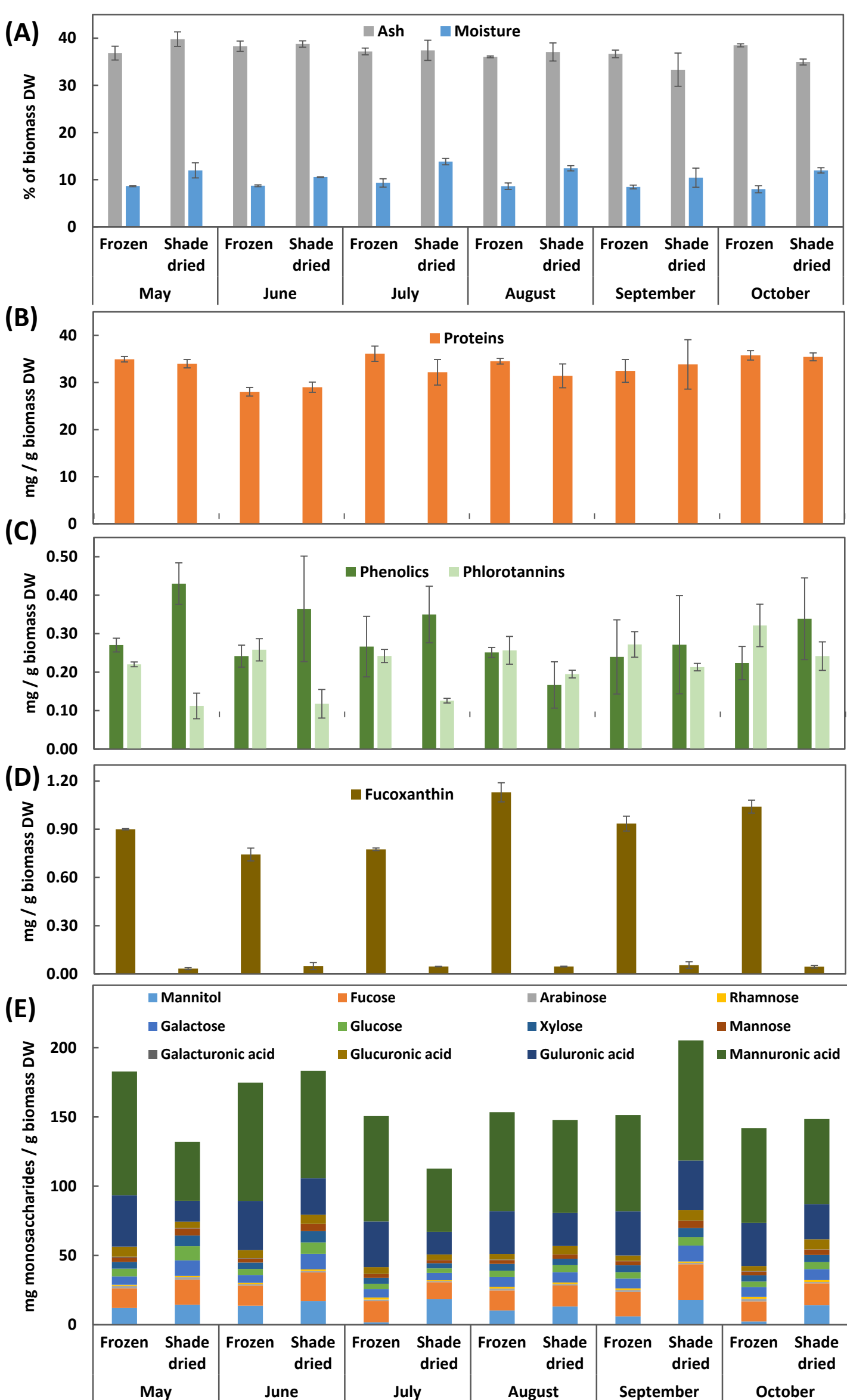**(B) from east of Jamaica; mean age (days)**
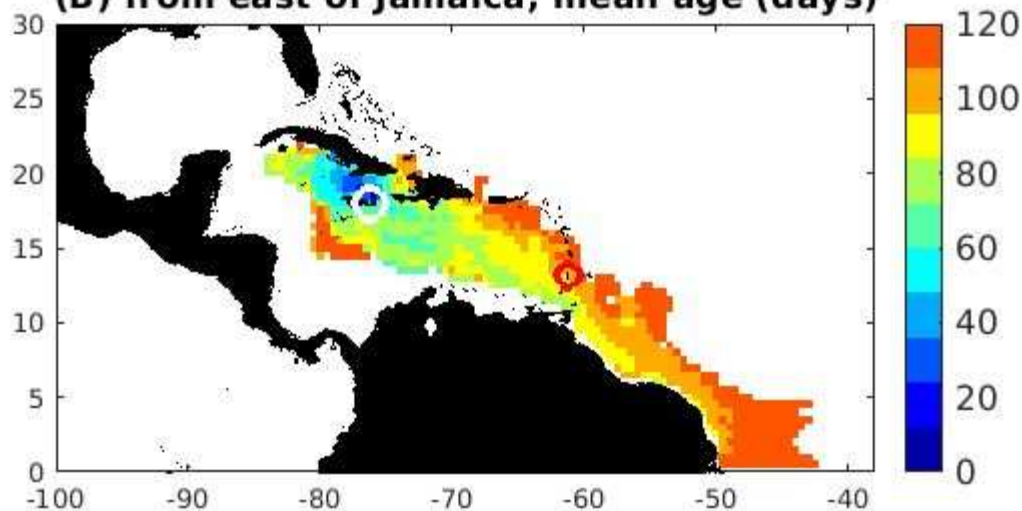
Figure 4.

Figure 5.

Figure 6.